FROM ELASTIC SCATTERING TO CENTRAL EXCLUSIVE PRODUCTION IN PROTON–PROTON COLLISIONS AT RHIC

Włodek Guryn[†]

Czech Technical University, Prague, Czech Republic

Received 1 April 2026, accepted 17 April 2026, published online 28 May 2026

We describe the physics program at the Relativistic Heavy Ion Collider (RHIC) with forward protons measured in the Roman Pot system. The program started as a standalone PP2PP experiment with a goal of measuring of proton–proton elastic scattering. The PP2PP experiment took data at RHIC as a dedicated experiment at the beginning of RHIC operations. To expand the physics program to include non-elastic channels with forward protons, such as Central Exclusive Production (CEP), Central Production (CP), and Single Diffraction Dissociation (SD), the experiment with its equipment was merged with the STAR experiment at RHIC. This allowed for a more comprehensive diffractive physics program with measured forward protons. The expanded program, which included both elastic and inelastic proton–proton scattering, became part of the physics program and operations of the STAR experiment. The results obtained by both programs are described here. Given that proton beams at RHIC were polarized, the results include spin dependence in proton–proton elastic scattering.

DOI:10.5506/APhysPolB.57.6-A11

1. Introduction

It is my honor to deliver this lecture at the 66$^{\text{th}}$ Cracow School of Theoretical Physics in honor of Prof. Andrzej Białas's 90$^{\text{th}}$ birthday. The Cracow School of Theoretical Physics, which I attended a few times, was a great place to meet and interact with many colleagues. In particular, the discussions with Prof. Białas were very insightful and had a great impact on my work, for which I thank him very much.

In the description of the physics program, we follow the timeline and evolution of the program from its inception as a proton–proton elastic scattering experiment, PP2PP [1], to the most recent results with the STAR

[†] Brookhaven National Laboratory — retired.

experiment [2], where the program was expanded to include more diffractive physics topics, taking advantage of the STAR experiment's coverage in the central rapidity region.

The program with STAR included topics such as Centra Exclusive Production (CEP), Central Production (CP), Single Diffractive Dissociation (SDD), and a more precise measurement of both spin-averaged proton–proton elastic scattering and its spin dependence, which we were able to investigate due to the polarized-proton beams at RHIC.

2. The PP2PP Experiment

In addition to a well-motivated program of proton–proton elastic scattering at RHIC, at the time of the formulation of the RHIC physics program, there was a puzzle in the ρ-value measurement, see definition Eq. (3), by the UA4 experiment [3] at the S$p\bar{p}$S collider at CERN at $\sqrt{s} = 546$ GeV. The UA4 measured value of $\rho = 0.24$ was well above the expected value of $\rho \approx 0.12$. Hence, it was quite natural to propose an experiment at RHIC at $\sqrt{s} = 510$ GeV [4], which among other observables in elastic scattering, could measure the ρ value in proton–proton collisions at a similar to UA4 experiment's $\sqrt{s}$. Furthermore, at the time of the proposal, the $\sqrt{s} = 510$ GeV would have been the highest proton–proton collision energy. Hence, a comprehensive experiment to measure total and elastic cross sections was proposed for the RHIC physics program.

We start by introducing basic quantities needed to describe elastic scattering. The proton–proton elastic scattering, Fig. 1, is described by a scattering amplitude which has two components: the electromagnetic part, described by the well-known Coulomb amplitude f_c, and the hadronic part, described by the hadronic amplitude f_h. The hadronic amplitude is commonly expressed as a function of center-of-mass energy $\sqrt{s}$ and four-momentum-transfer squared t, which for small scattering angles θ can be expressed as

$$t = (p_{\text{in}} - p_{\text{out}})^2 \approx -p^2\theta^2 = -p^2 \left(\theta_x^2 + \theta_y^2\right) . \tag{1}$$

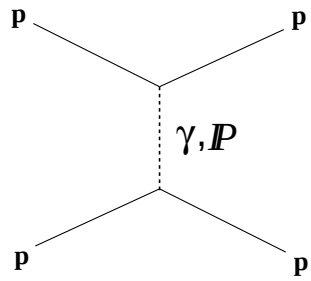

Fig. 1. Diagram of pp elastic scattering.

The differential elastic pp cross section is expressed as a square of the scattering amplitude

$$\frac{\mathrm{d}\sigma_{\mathrm{el}}}{\mathrm{d}t} = \pi |f_c + f_h|^2 \,. \tag{2}$$

Thus, the differential cross section $\mathrm{d}\sigma_{\mathrm{el}}/\mathrm{d}t$ of elastic scattering at small angles is determined by Coulomb and nuclear amplitudes and the interference term between them. The cross section is given by [5]

$$\begin{aligned} \frac{\mathrm{d}\sigma_{\mathrm{el}}}{\mathrm{d}t} \;=\; & 4\,\pi\,(\hbar c)^2 \left(\frac{\alpha\, G_{\mathrm{E}}^2}{t}\right)^2 + \frac{1+\rho^2}{16\,\pi\,(\hbar c)^2}\,\sigma_{\mathrm{tot}}^2\,\mathrm{e}^{-B\,|t|} \\ & -(\rho + \Delta\Phi)\,\frac{\alpha\, G_{\mathrm{E}}^2}{|t|}\,\sigma_{\mathrm{tot}}\,\mathrm{e}^{-\frac{1}{2}B\,|t|}\,, \end{aligned} \tag{3}$$

where α is the fine structure constant, G_{E} is the electric form factor of the proton, $\Delta\Phi$ is the Coulomb phase [6], ρ is the ratio of the real-to-imaginary part of the forward scattering amplitude, σ_{tot} is the total cross section, and B is the nuclear slope parameter. The first term in Eq. (3) is the Coulomb term, the second is the hadronic term, and the third is the so-called Coulomb Nuclear Interference (CNI) term.

2.1. Spin dependence in elastic scattering

Spin-depenedent proton–proton elastic scattering with transversely polarized beams is described by five independent helicity amplitudes ϕ_i [7]. Each of the amplitudes has hadron and Coulomb terms: $\phi_i = \phi_i^{\mathrm{em}} + \phi_i^{\mathrm{had}}$, where the Coulomb part is calculable in QED. The observables — total cross section σ_{tot}, differential elastic cross section $\frac{\mathrm{d}\sigma}{\mathrm{d}t}$, single spin analyzing power A_N, and other spin-dependent quantities — can be derived from the helicity amplitudes ϕ_i [7].

3. Results from the PP2PP experiment

We start with a brief description of the setup. The protons, which scatter elastically at small angles (few mrad), move inside the beam pipe and follow the optics of the RHIC magnets. They are measured by a system of Si strip detectors placed close to the beam inside movable vessels known as Roman Pots (RPs) [1]. The layout of the experiment is shown in Fig. 2.

The PP2PP experiment published three results on pp elastic scattering at $\sqrt{s} = 200$ GeV. They are shown in Fig. 3 and Table 1. These were the first results from pp elastic scattering above the ISR $\sqrt{s}$ of 63 GeV, the highest $\sqrt{s}$ at the time. The first result was the measurement of the B-slope [8] parameter, see Eq. (3).

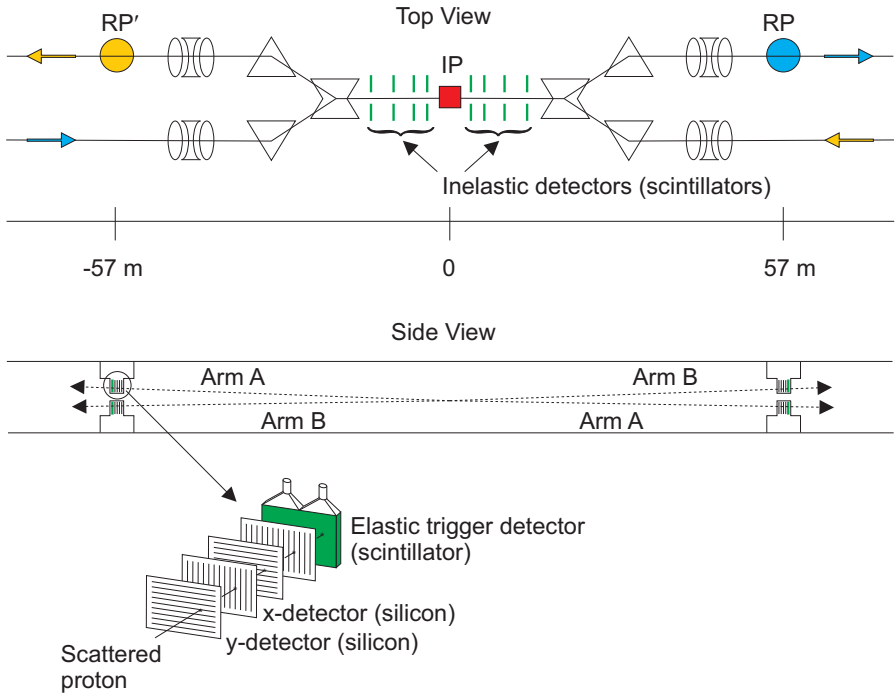

Fig. 2. The layout of the PP2PP experiment. The location of the RPs at about 55 m from the IP and the details of the detecor package are shown.

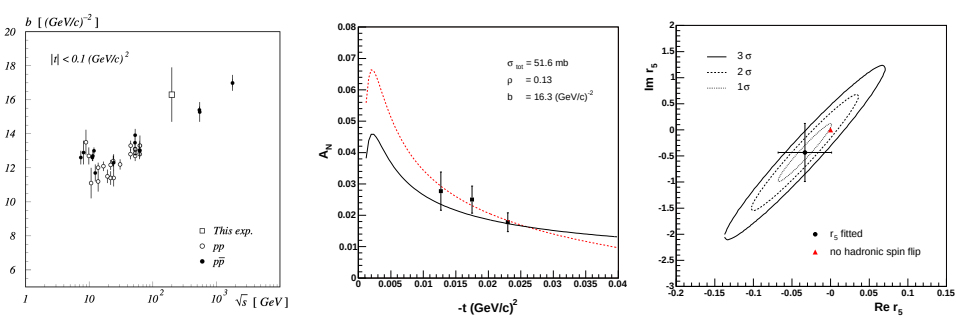

Fig. 3. Results from the PP2PP experiment: B-slope (left), A_N (middle), and $\mathrm{Im}(r_5)$ *versus* $\mathrm{Re}(r_5)$ (right) are shown.

It was measured in the small t-range $0.010 \leq -t \leq 0.019$ GeV^2 to be $B = 16.3 \pm 1.6(\mathrm{stat.}) \pm 0.9(\mathrm{syst.})$ GeV^{-2}. The error bars were rather large due to the limited statistics of the measurement. Spin dependence in pp elastic scattering was also measured. Both the single spin asymmetry A_N [9]

Table 1. Double spin asymmetries A_{NN}, A_{SS}, $(A_{NN}+A_{SS})/2$, and $(A_{NN}-A_{SS})/2$ for the t-interval $0.010 \leq -t \leq 0.030$ $(\mathrm{GeV}/c)^2$ at $\langle -t \rangle = 0.0185$ $(\mathrm{GeV}/c)^2$.

	A_{NN}	A_{SS}	$(A_{NN}+A_{SS})/2$	$(A_{NN}-A_{SS})/2$
Asym	0.0298	0.0035	0.0167	0.0131
ΔAsym (stat.+norm.)	$\pm$0.0166	$\pm$0.0081	$\pm$0.0091	$\pm$0.0096
ΔAsym (syst.)	$\pm$0.0045	$\pm$0.0031	$\pm$0.0034	$\pm$0.0072
ΔAsym due to $\Delta(P_Y \cdot P_B)$			$\pm$32.3%	

and double spin asymmetry A_{NN} [10] were measured in the low-t region, $0.002 < -t < 0.03$ GeV^2. The A_N in this t-range is sensitive to a possible contribution from the hadronic spin-flip amplitude, which is due to the interference of the Pomeron spin-flip amplitude and electromagnetic non-flip amplitude, and would change A_N. The common measure of this effect is the variable r_5 [7, 11], which measures the ratio of hadronic spin-flip to non-flip amplitudes. It was found that A_N follows the Coulomb Nuclear Interference curve and that the r_5 fitted to the data was compatible with no hadronic spin-flip. The double-spin asymmetry A_{NN} was also found to be compatible with zero.

4. Results on elastic scattering at STAR

As mentioned earlier, the Roman Pot setup of the PP2PP experiment was subsequently moved to and became part of the STAR to continue the pp elastic scattering program and also to expand the physics program to include diffractive scattering with measured forward protons. We start with the results on elastic pp scattering.

The first is an improved result on the A_N at $\sqrt{s} = 200$ GeV [12]. It put a more stringent limit on the hadronic spin-flip amplitude r_5 using higher statistics data in the t-range $0.003 \leq -t \leq 0.035$ GeV^2, where there is a significant interference between the electromagnetic and hadronic scattering amplitudes. The measured values of A_N and its t-dependence are consistent with a vanishing hadronic spin-flip amplitude within 1σ, see Fig. 4, where the real and imaginary parts of r_5 are plotted. The measurement provides a strong constraint on the ratio of the single spin-flip to the non-flip amplitudes. Since the hadronic amplitude is dominated by the Pomeron amplitude at this $\sqrt{s}$, it provides a strong constraint on the presence of a hadronic spin flip due to the Pomeron exchange in polarized pp elastic scattering.

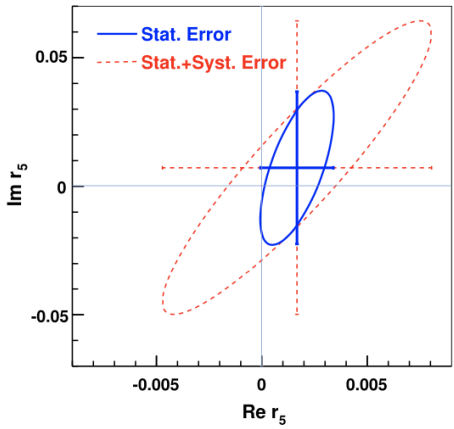

Fig. 4. Fitted value of r_5, Im r_5 *versus* Re r_5, with contours corresponding to statistical error (solid ellipse and cross) and statistical+systematic errors added in quadrature (dashed ellipse and cross) of 1σ.

The second is a measurement of the elastic differential cross section at $\sqrt{s} = 200$ GeV measured in the t-range $0.045 \leq -t \leq 0.135$ GeV^2 [13], see Fig. 5 (left). The results included the following observables. The total cross section $\sigma_{\rm tot}$, obtained from extrapolation of the $\mathrm{d}\sigma/\mathrm{d}t$ to the optical point at $t = 0$, is $\sigma_{\rm tot} = 54.67 \pm 0.21(\text{stat.})^{+1.28}_{-1.38}(\text{syst.})$ mb. The value of the exponen-

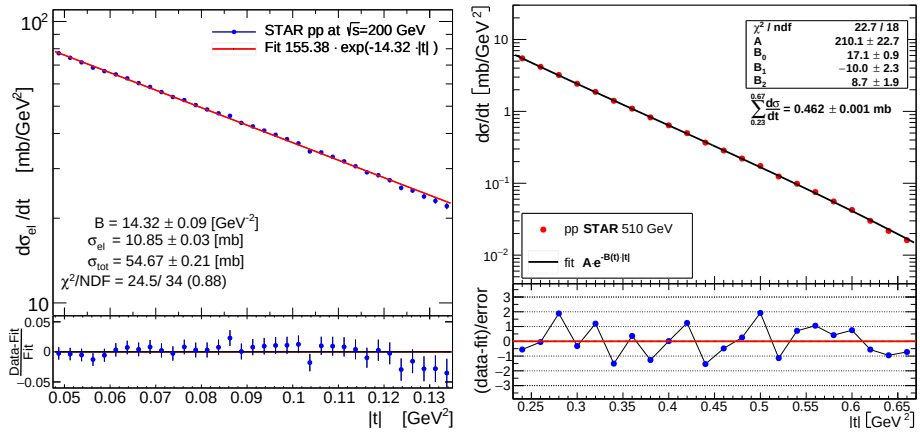

Fig. 5. The pp elastic differential cross section $\mathrm{d}\sigma/\mathrm{d}t$. Left: results at $\sqrt{s} = 200$ GeV [13] fitted with exponential $Ae^{-B|t|}$. Right: results at $\sqrt{s} = 510$ GeV [14] fitted with exponential $Ae^{B(t)|t|}$. Results are shown in the top panels, respectively; residuals (Data−Fit)/Fit are shown in the bottom panels, respectively. Uncertainties are statistical only.

tial slope parameter B of the elastic differential cross section $\mathrm{d}\sigma/\mathrm{d}t \sim \mathrm{e}^{-Bt}$ in the measured t-range is $B = 14.32 \pm 0.09(\mathrm{stat.})^{+0.13}_{-0.28}(\mathrm{syst.})$ GeV^{-2}, the values of the elastic cross section is $\sigma_{\mathrm{el}} = 10.85 \pm 0.03(\mathrm{stat.})^{+0.49}_{-0.41}(\mathrm{syst.})$ mb, the elastic cross section integrated within the STAR t-range to be $\sigma_{\mathrm{el}}^{\mathrm{det}} = 4.05 \pm 0.01(\mathrm{stat.})^{+0.18}_{-0.17}(\mathrm{syst.})$ mb, and the inelastic cross section is $\sigma_{\mathrm{inel}} = 43.82 \pm 0.21(\mathrm{stat.})^{+1.37}_{-1.44}(\mathrm{syst.})$ mb. The result on σ_{tot} is the only one on the total cross section at $\sqrt{s}$ between the ISR and the LHC energies. All the results agree well with the world data.

The third is the measurement of elastic scattering at $\sqrt{s} = 510$ GeV in the t-range $0.23 \leq -t \leq 0.67$ GeV^2 [14], see Fig. 5 (right). This is the only measurement of the proton–proton elastic cross section in this t-range for collision energies above the ISR and below the LHC colliders. It is found that a constant exponential slope B does not fit the data in the aforementioned t range, and that a much better fit is obtained using a second-order polynomial for $B(t)$. This is the first measurement below the LHC energies for which the non-constant behavior $B(t)$ is observed. The integrated elastic cross section within the STAR t-range is found to be $\sigma_{\mathrm{el}}^{\mathrm{fid}} = 462.1 \pm 0.9(\mathrm{stat.}) \pm 1.1(\mathrm{syst.}) \pm 11.6(\mathrm{scale})$ μb.

5. Results on Central Exclusive Production at STAR

As mentioned earlier, the major motivation to move the Roman Pot system to STAR was a possibility of combining the measurement of the forward protons with the measurement of the central (recoil) system in the STAR detector, thus allowing for the determination of the exclusivity of the final state in the $pp \to pXp$ reaction, where all the particles in the final are measured, see Fig. 6.

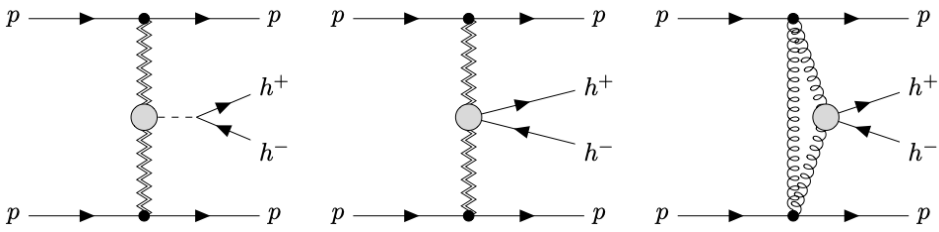

Fig. 6. Diagrams of CEP of h^+h^- in the DPE process. The resonant (left) and continuum production (middle) are shown. The two-gluon approximation of continuum production in DPE in perturbative QCD (right) is also shown. The Pomerons are represented by double zigzag lines and gluons by spiral lines.

The verification of the exclusivity of that final state is a very unique feature of the results described here. This is contrary to other measurements where exclusivity is inferred by requiring a rapidity gaps and a small p_{T} of the final state. The latter is a reasonable approximation of the exclusivity but it is clearly not the same as the measurement of all particles in the final state. In the results described here, the system X consists of hadron pairs of opposite charge $\pi^+\pi^-$, K^+K^-, and $p\bar{p}$.

The charged particle pairs' momenta are obtained from the tracks measured in the Time Projection Chamber (TPC) of the central detector. The particle identification (PID) is obtained using the energy loss ($\mathrm{d}E/\mathrm{d}x$) measured in the TPC and the time-of-flight measurement in the Time-of-Flight (TOF) system. The momenta of forward-scattered protons are reconstructed using measurements in the Roman Pot system.

Exclusivity of the event is determined by requiring the transverse momentum balance of all four final-state particles to have small missing transverse momentum, $p_{\mathrm{T}}^{\mathrm{miss}}$. At $\sqrt{s} = 200$ GeV, $p_{\mathrm{T}}^{\mathrm{miss}} < 75$ MeV/c and at $\sqrt{s} = 510$ GeV, $p_{\mathrm{T}}^{\mathrm{miss}} < 120$ MeV/c.

The number of differential cross sections is measured in the fiducial volume of the STAR detector, as a function of various observables of the central hadronic final state and of the forward-scattered protons. Representative results at $\sqrt{s} = 200$ GeV and $\sqrt{s} = 510$ GeV are described in the following subsections.

The phenomenological interpretation of the data requires improvements of the DPE models to consistently include the continuum and resonance-production mechanisms, and the interference between the two, as well as absorption and re-scattering effects.

5.1. Results on CEP at $\sqrt{s} = 200$ GeV

We present a brief summary of the results obtained at $\sqrt{s} = 200$ GeV, for a more detailed discussion, see [15]. The fiducial region roughly corresponds to t-values at the proton vertices (t_1, t_2), in the range $0.04 < -t_1, -t_2 < 0.2$ GeV^2, invariant masses M_X of the charged hadron pairs up to a few GeV, and pseudorapidities (η) of the centrally-produced hadrons to be in the acceptance of the TOF system's acceptance $|\eta| < 0.7$.

In Fig. 7, the measured differential cross section within STAR acceptance, as a function of invariant mass distribution M_X of the central system for $\pi^+\pi^-$, K^+K^-, and $p\bar{p}$ is shown. The mass spectrum of the $\pi^+\pi^-$ pairs shows a drop at ~ 1.0 GeV, a clear peak at ~ 1.3 GeV, which is consistent with $f_2(1270)$ resonance, and possible further structures at higher masses. The predictions from various Double Pomeron Exchange (DPE) production models of continuum of hadron pairs is also shown.

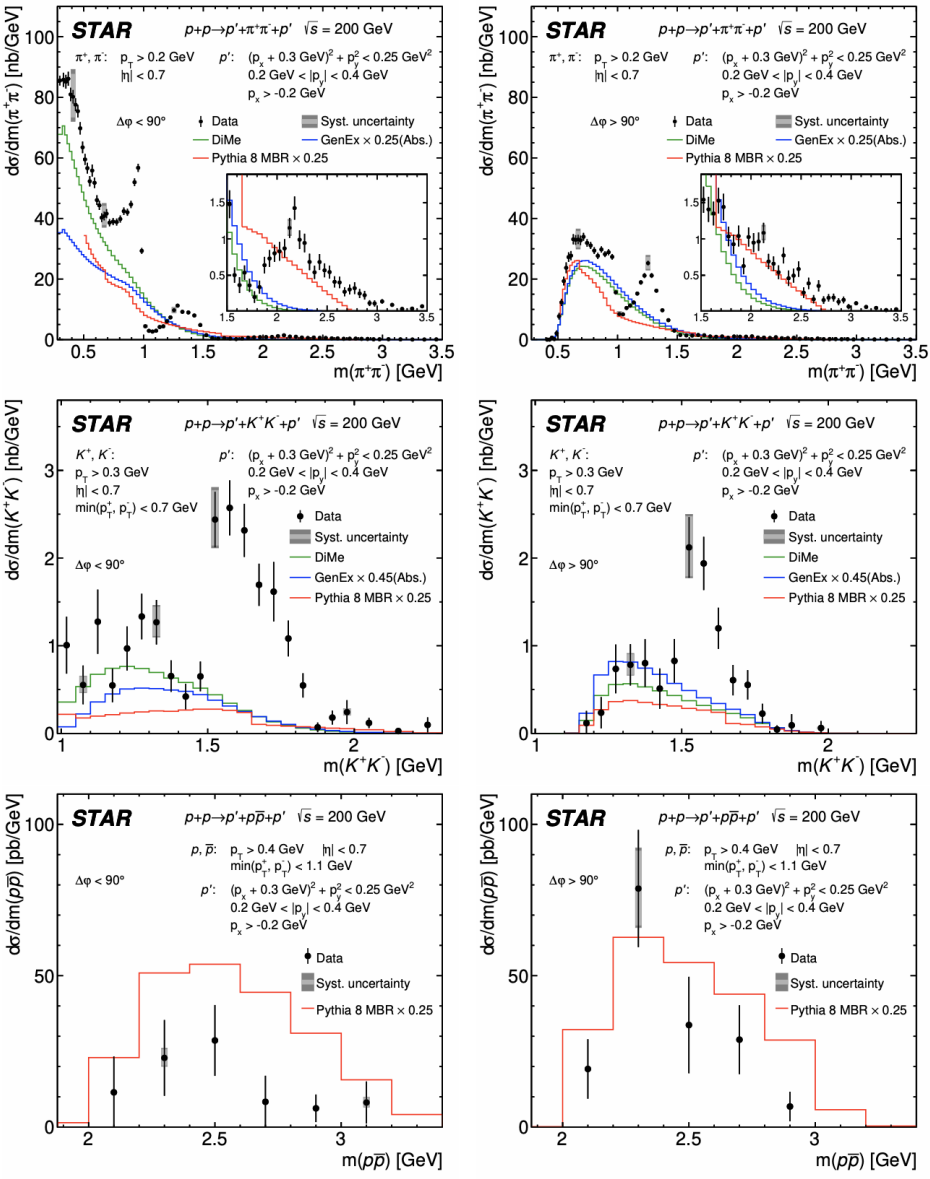

Fig. 7. Differential cross sections for CEP of charged particle pairs $\pi^+\pi^-$ (top), K^+K^- (middle), and $p\bar{p}$ (bottom) as a function of the invariant mass of the pair in two $\Delta\phi$ regions, $\Delta\phi < 90°$ (left column) and $\Delta\phi > 90°$ (right column), measured in the fiducial region explained on the plots. Data are shown as solid points with error bars representing the statistical uncertainties.

In Fig. 8, the differential cross section $\mathrm{d}\sigma/\mathrm{d}m_{\pi^+\pi^-}$ of the invariant mass of $\pi^+\pi^-$ system extrapolated from the fiducial region to the Lorentz-invariant phase space given by the central-state rapidity, $|y_{\pi^+\pi^-}| < 0.4$, and t of the froward protons $0.05 < t_1, t_2 < 0.16$ GeV^2 is shown. The extrapolated cross section is well described by the continuum production with at least three resonances, the $f_0(980)$, $f_2(1270)$ and $f_0(1500)$, with a possible small contribution from the $f_0(1370)$.

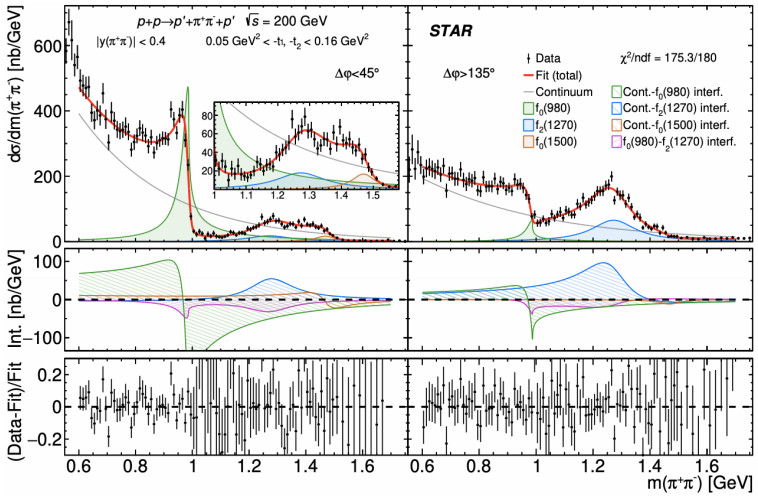

Fig. 8. The left and right columns show the cross sections for $\Delta\phi < 45°$ and $\Delta\phi > 135°$, respectively. The data are shown as black points with error bars representing statistical uncertainties. The result of the fit, $F(m)$, is drawn with a solid red line. The squared amplitudes for the continuum and resonance production are drawn with lines of different colors, as explained in the legend. The most significant interference terms are plotted in the middle panels, while the relative differences between each data point and the fitted model are shown in the bottom panels.

The masses and widths of the $f_0(980)$ and $f_0(1500)$ resonances obtained from the fit are in good agreement with the PDG values.

The two scalar mesons, $f_0(980)$ and $f_0(1500)$, are produced predominantly at $\Delta\phi > 45°$, whereas the tensor meson $f_2(1270)$ is predominantly produced at $\Delta\phi > 135°$. This $\Delta\phi$ dependence is consistent with the observation made by the WA102 Collaboration [16].

5.2. Results on CEP at $\sqrt{s} = 510$ GeV

We present a brief summary of the results obtained at $\sqrt{s} = 510$ GeV, for a more detailed discussion, see [17]. This is the first measurement of the

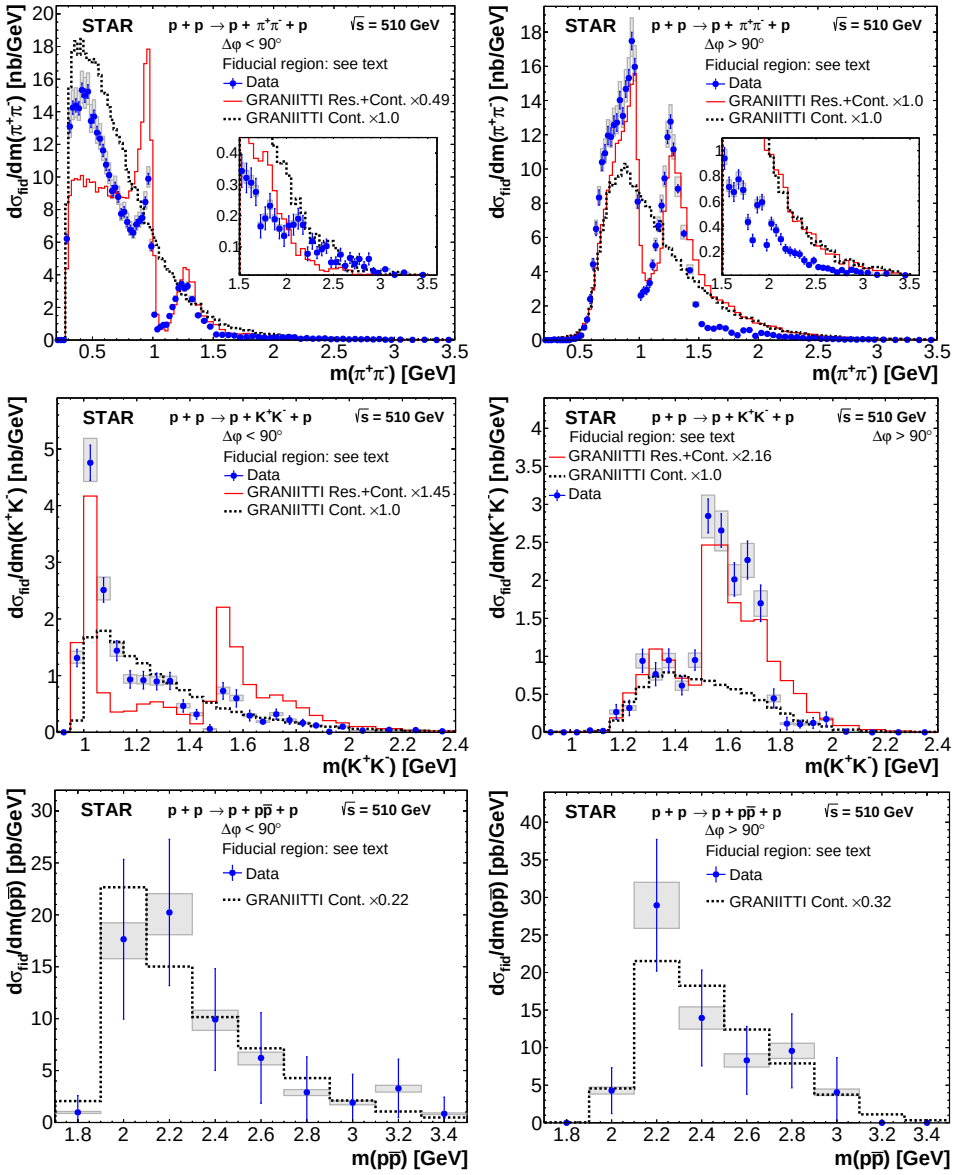

Fig. 9. The invariant mass M_x distributions of $\pi^+\pi^-$(top), K^+K^- (center) and $p\bar{p}$ (bottom) for CEP at $\sqrt{s} = 510$ GeV. In the left column, mass distributions for $\Delta\varphi < 90°$ and in the right column, $\Delta\varphi > 90°$ are shown. Results are compared with the GRANIITTI Monte Carlo.

CEP process in proton–proton collisions: $pp \to ph^+h^-p$ at that $\sqrt{s}$. The differential fiducial cross sections are presented as a function of the difference in the azimuthal angle between the outgoing protons. They include the invariant masses of the charged hadron pairs, see Fig. 9, which are measured up to ~ 3 GeV and the square of the four-momentum transfer of the two forward-scattered protons in the range $0.3\ \text{GeV}^2 < -t_1, -t_2 < 1.6\ \text{GeV}^2$. The observed spectra are consistent with double Pomeron exchange, including resonances seen in previous studies, while the possible $f_0(980)$ resonance is reported here for the first time in the K^+K^- decay channel.

6. Other unpublished, interesting results

In this section, two interesting unpublished topics are presented.

6.1. Particle production in CD and SD processes at STAR

The next set of results was obtained on particle production in central production (CP) and single diffraction dissociation (SD) processes [18]. The SD process, where one proton stays intact, is $pp \to p + X$, while in the CD process $pp \to p + X + p$, both protons stay intact after the collision. In both cases, X denotes a diffractively produced system in the center of rapidity. An important characteristic is that there is a rapidity gap between the forward protons and the system X. Particle interactions are typically described by QCD-inspired models implemented in Monte Carlo event generators with free parameters that can be constrained by diffractive measurements. Hence, these processes provide insight into the non-perturbative regime of QCD.

Among the results that were obtained were measurements of inclusive charged-particle distributions and identified particle/antiparticle ratios as a function of transverse momentum p_{T} and η in CD and SD processes.

In Fig. 10, charged particle multiplicities n_{ch} are shown, while in Fig. 11, the p_{T} distributions are shown. In both cases, good agreement with the PYTHIA 8 MC generator is shown.

6.2. Diffractive production of J/Ψ

Diffractive production of J/Ψ is also measured as presented at the Diffraction and Low-x conference [19]. The schematic diagram of the process is shown in Fig 12. The data were acquired using a calorimeter trigger to obtain the J/Ψ data sample. Among those triggers, events with a proton measured in one of the RPs are selected.

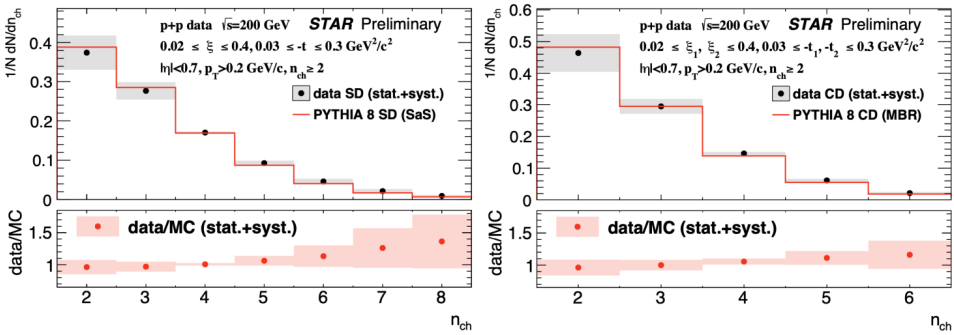

Fig. 10. Multiplicity distributions of primary charged particles for SD (left) and CD (right) processes. Data are compared to PYTHIA 8 simulations.

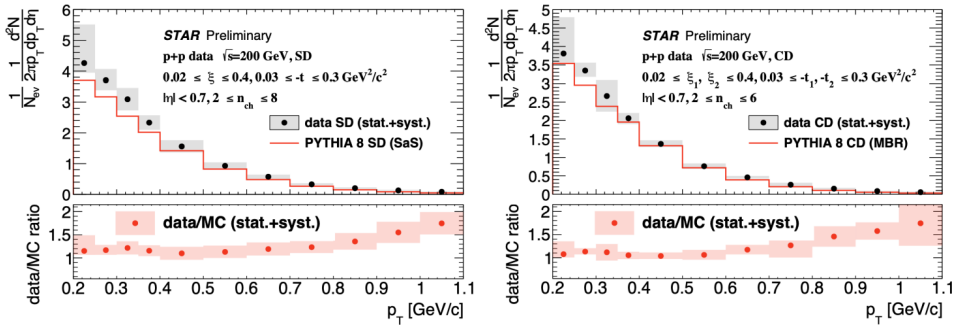

Fig. 11. Charged particle rates as a function of transverse momentum for SD (left) and CD (right) processes. Data are compared to PYTHIA 8 MC simulations.

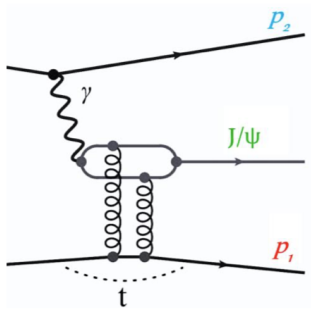

Fig. 12. Schematic of the J/Ψ production. One proton p_1 at the gluon vertex is measured in the RP system, the other proton p_2 at the photon vertex scatters at a small angle is not measured. The $J/\Psi \Rightarrow e^+e^-$ is measured in the calorimeter.

The events in the J/Ψ mass range with a proton measured in one RP are shown in Fig. 13 on the left. The missing p_{T} of the events in the J/Ψ mass range is shown on the right of Fig 13. The peak near $p_{\mathrm{T}} = 0$ in the region labeled A is consistent with the J/Ψ exclusive production.

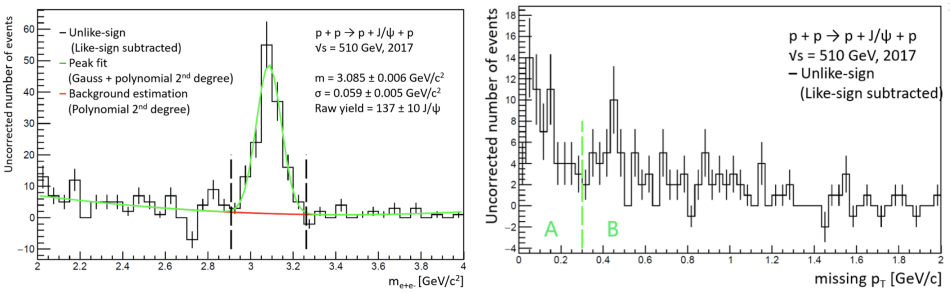

Fig. 13. Invariant mass distribution of e^+e^- pairs and the missing p_{T} of the events in the J/Ψ mass range.

7. Summary

We have presented a rich physics program with measured forward protons at RHIC, which includes topics on a number of diffractive processes: elastic scattering, SD, CEP, and CP. This specialized program used unique features of the RHIC complex, including polarized proton beams. There were three publications from the PP2PP experiment and five publications from the STAR experiment. Also, five Ph.D. theses and nine M.Sc. theses were written based on this program.

The author is deeply grateful to his PP2PP and STAR experiment colleagues whose work led to the results described here. Since list is long, I regret that I cannot acknowledge everyone by name here.

Of the major contributors, first, I thank those colleagues from the PP2PP experiment without whom nothing would have been accomplished: Prof. S. Bültmann, whose hands-on work and thoughtful insights were most crucial; C. Pearson, the talented engineer who designed the RP system; Dr. D. Lynn for his clever SSDs design; Prof. M. Rijssenbeek for his all-around work on the experiment's every aspect, and Drs. I. Alekseev and D. Svirida for their crucial work on electronics.

Second, I give thanks to the team led by Dr. L. Adamczyk, Prof. J. Chwastowski. Dr. B. Pawlik, and Prof. M. Przybycień for significant contributions in all phases of this program. My thanks go as well to five Ph.D. students for their fine analyses of this physics: Drs. D. Plyku, L. Fulek, I. Koralt, R. Sikora, and T. Truhlář. I also give my gratitude to Dr. J. Bielčík for his hospitality during this review's writing.

Last but not least, I am most appreciative of the late Dr. S. Aronson, without whose support and encouragement this work would not have been possible.

My work was supported by the Office of Nuclear Physics within the Office of Science of the U.S. Department of Energy and the Ministry of Education, Youth and Sports of the Czech Republic.

REFERENCES

[1] PP2PP Collaboartion (S. Bültmann *et al.*), «The PP2PP experiment at RHIC: silicon detectors installed in Roman Pots for forward proton detection close to the beam», *Nucl. Instrum. Methods Phys. Res. A* **535**, 415 (2004).

[2] K.H. Ackermann *et al.*, «STAR detector overview», *Nucl. Instrum. Methods Phys. Res. A* **499**, 624 (2003).

[3] UA4 Collaboartion (D. Bernard *et al.*), «The real part of the proton–antiproton elastic scattering amplitude at the centre of mass energy of 546 GeV», *Phys. Lett. B* **198**, 583 (1987).

[4] W. Guryn *et al.*, RHIC Proposal R7, 1994 (unpublished).

[5] U. Amaldi *et al.*, «Measurements of the proton–proton total cross section by means of Coulomb scattering at the CERN intersecting storage rings», *Phys. Lett. B* **43**, 231 (1973).

[6] B.Z. Kopeliovich, A.V. Tarasov, «The Coulomb phase revisited», *Phys. Lett. B* **497**, 44 (2001).

[7] N.H. Büttimore *et al.*, «Spin dependence of high energy proton scattering», *Phys. Rev. D* **59**, 114010 (1999).

[8] PP2PP Collaboartion (S. Bültmann *et al.*), «First measurement of proton–proton elastic scattering at RHIC», *Phys. Lett. B* **579**, 245 (2004).

[9] PP2PP Collaboartion (S. Bültmann *et al.*), «First measurement of A_N at $\sqrt{s_{NN}} = 200$ GeV in polarized proton–proton elastic scattering at RHIC», *Phys. Lett. B* **632**, 167 (2006).

[10] PP2PP Collaboartion (S. Bültmann *et al.*), «Double spin asymmetries A_{NN} and A_{SS} at $\sqrt{s_{NN}} = 200$ GeV in polarized proton–proton elastic scattering at RHIC», *Phys. Lett. B* **647**, 98 (2007).

[11] B.Z. Kopeliovich, B.G. Zakharov, «Spin-flip component of the pomeron», *Phys. Lett. B* **226**, 156 (1989).

[12] STAR Collaboration (L. Adamczyk *et al.*), «Single spin asymmetry A_N in polarized proton–proton elastic scattering at $\sqrt{s_{NN}} = 200$ GeV», *Phys. Lett. B* **719**, 62 (2013).

[13] STAR Collaboration (J. Adam *et al.*), «Results on total and elastic cross sections in proton–proton collisions at $\sqrt{s_{NN}} = 200$ GeV», *Phys. Lett. B* **808**, 135663 (2020).

[14] STAR Collaboration (J. Adam *et al.*), «Results on elastic cross sections in proton–proton collisions at $\sqrt{s_{NN}} = 510$ GeV with the STAR detector at RHIC», *Phys. Lett. B* **852**, 138601 (2024).

[15] STAR Collaboration (J. Adam *et al.*), «Measurement of the central exclusive production of charged particle pairs in proton–proton collisions at $\sqrt{s_{NN}} = 200$ GeV with the STAR detector at RHIC», *J. High Energy Phys.* **2020**, 178 (2020).

[16] WA102 Collaboration (D. Barberis *et al.*), «Experimental evidence for a vector-like behaviour of Pomeron exchange», *Phys. Lett. B* **467**, 165 (1999).

[17] STAR Collaboration (T. Truhlar), «Study of the central exclusive production of $\pi^+\pi^-$, K^+K^- and $p\bar{p}$ pairs in proton–proton collisions at $\sqrt{s} = 510$ GeV with the STAR detector at RHIC», arXiv:2012.06295 [hep-ex].

[18] STAR Collaboration (L. Fulek), «Measurements of Particle Spectra in Diffractive Proton–Proton Collisions with the STAR Detector at RHIC», *Acta Phys. Pol. B Proc. Suppl.* **12**, 999 (2019).

[19] STAR Collaboration (M. Sverakova), talk at the Diffraction and Low-x 2024, September 8–14, 2024, Palermo, Sicily, Italy.